Organic-Inorganic Hybrid Cuprous-Based Metal Halides with Unique Two-Dimensional Crystal Structure for White Light-Emitting Diodes

Xuan Meng, Junke Jiang, Xinyu Yang, Hongyuan Zhao, Qichao Meng, Yunfei Bai, Qiujie Wang, Jitao Song, Claudine Katan, Jacky Even, et al.

Organic-Inorganic Hybrid Cuprous-Based Metal Halides with Unique 2D Crystal Structure

Xuan Meng,[1] Xinyu Yang,[1] Hongyuan Zhao,[1] Qichao Meng,[1] Yunfei Bai,[1] Qiujie Wang,[1] Jitao Song,[1] Junke Jiang,[2] Claudine Katan,[3] Jacky Even,*[,2] Feng Liu,*[,1] William W. Yu*[,4]

[1]Institute of Frontier Chemistry, School of Chemistry and Chemical Engineering, Shandong University, Qingdao 266237, China

[2]Univ Rennes, INSA Rennes, CNRS, Institut FOTON - UMR 6082, F-35000 Rennes, France

[3]Univ Rennes, ENSCR, CNRS, ISCR-UMR 6226, F-35000 Rennes, France

[4]School of Chemistry and Chemical Engineering; Key Laboratory of Special Functional Aggregated Materials, Ministry of Education; Shandong Key Laboratory of Advanced Organosilicon Materials and Technologies, Shandong University, Jinan 250100; Shandong Provincial Key Laboratory for Science of Material Creation and Energy Conversion, Science Center for Material Creation and Energy Conversion, Shandong University, Qingdao 266237, China

*E-mails: jacky.even@insa-rennes.fr (J. Even); fenglau189@sdu.edu.cn (F. Liu); wyu6000@gmail.com (W. W. Yu)

Abstract

Ternary cuprous (Cu^+)-based metal halides, represented by $CsCu_2I_3$ and $Cs_3Cu_2I_5$, are garnering increasing interest for light-emitting applications owing to their intrinsically high photoluminescence quantum yield and direct bandgap. Toward electrically driven light-emitting diodes (LEDs), it is highly desirable for the light emitters to have a high structural dimensionality as it may favor efficient electrical injection. However, unlike lead-based halide perovskites whose light-emitting units can be facilely arranged in three-dimensional (3D) ways, to date, nearly all ternary Cu^+-based metal halides crystallize into 0D or 1D networks of Cu-X (X = Cl, Br, I) polyhedra, whereas 3D and even 2D structures remain mostly uncharted. Here, by employing a fluorinated organic cation, we report a new kind of ternary Cu^+-based metal halides, (DFPD)CuX_2 ($DFPD^+$ = 4,4-difluoropiperidinium), which exhibits unique 2D layered crystal structure. Theoretical calculations reveal a highly dispersive conduction band of (DFPD)$CuBr_2$, which is beneficial for charge carrier injection. It is also of particular significance to find that the 2D (DFPD)$CuBr_2$ crystals show appealing properties, including improved ambient stability and an efficient warm white-light emission, making it a promising candidate for single-component lighting and display applications.

Keywords: lead-free metal halide; electrically driven LED; 2D crystal structure; cuprous luminescence

Introduction

The past few years have witnessed significant breakthroughs in the field of lead (Pb)-based metal halides and their efficient use in photovoltaics and light-emitting diodes (LEDs). Nowadays, power conversion efficiency of the small-area Pb-based perovskite solar cells has exceeded 25%;[1-3] LEDs based on Pb halide perovskites have demonstrated external quantum efficiencies (EQEs) over 20% (red: 25.8%,[4] green: 30.8%,[5] blue: 21.4%[6]). The high optoelectronic quality of Pb halide perovskites is believed to stem from their unique electronic band structure, which endows the

materials with suitable direct bandgap, strong optical absorption, small carrier effective masses, and high defect tolerance.[7, 8] However, large-scale use of Pb-based materials raises concern about their potential toxicity. Besides, most Pb perovskites suffer from poor stability against moisture originated from their soft and ionic nature, which may severely limit commercial prospects. For these reasons, significant research interest has been focused on developing new, stable Pb-free compounds with similar crystal and electronic structures.

Recently, environmental benign elements such as Mn^{2+}, Cu^{+}, Ag^{+}, Bi^{3+}, Sb^{3+}, and In^{3+} have been explored to replace Pb^{2+}, giving rise to a series of new compositions with fascinating properties that are derived from their peculiar structure.[9] Among various types of "perovskite-inspired" materials, particular attention is given to those ternary cuprous (Cu^{+})-based metal halides because of their distinctive features of direct bandgap, intrinsic high photoluminescence quantum yield (PLQY), and abundant resource of Cu precursors.[10] Encouragingly, rapid advances have been witnessed in the field of Cu^{+}-based LEDs. For example, electrically driven yellow LEDs based on $CsCu_2I_3$ thin films have demonstrated EQE over 1%;[11] By incorporating $CsCu_2I_3$ emitters in host molecules, Kim *et al.* further boosted EQE of these halide LEDs to 7.4%, which is comparable to those of the best performing yellow LEDs using Pb perovskites.[12, 13] Toward blue LEDs with emission wavelength approaching 460 nm, $Cs_3Cu_2I_5$ is among the most investigated composition owing to its near-unity PLQY and excellent air stability.[14, 15] In a study by Shan *et al.*, blue LEDs were fabricated using $Cs_3Cu_2I_5$ nanocrystals and exhibited an EQE of ~1.1% and a half-lifetime exceeding 100 hours.[16]

However, despite substantial progress, there is still great potential to be exploited in enhancing optoelectronic performance of these Cu^{+}-based luminescent materials. For example, some of the most obvious limitations are the low structural, and often electronic, dimensionalities. The aforementioned $Cs_3Cu_2I_5$ and $CsCu_2I_3$ adopt zero-

dimensional (0D) and 1D crystallographic structures, respectively; $Cs_3Cu_2Cl_5$ (0D/quasi-1D), $CsCu_2Cl_3$ (1D), $Cs_5Cu_3Cl_6I_2$ (1D), and Rb_2CuCl_3 (1D) are all low-dimensional materials at the structural level.[17] Besides, a series of recently reported organic-inorganic hybrid compositions, such as $(MA)_2CuCl_3$ ($MA^+ = CH_3NH_3^+$), (TBA)$CuBr_2$ (TBA = tetrabutylammonium cation), and (18-crown-6)$_2Na_2(H_2O)_3Cu_4I_6$, all take on a 0D structure.[18-21] Indeed, according to the investigation of Yan *et al.*, because of the high energy level of Cu 3d orbital, ternary Cu^+-based halides are more energetically favorable within 2-, 3- or 4-fold coordination, rather than 6-fold coordination, a prerequisite for forming stable network on a 3D structure.[22] It is worth noting that while low structural dimensionality is advantageous in achieving a high PLQY because strong quantum confinement would endow crystals with a stable excitonic resonance, the isolated networks of metal-halide octahedral units can also lead to low carrier mobility and carrier injection from the electrical contacts to the emissive thin layers. This exacerbates problems with inefficient charge injection in LED devices and hinders further improvement in their electroluminescence (EL) performance. It is well understood that high structural dimensionality (2D or 3D) is often a prerequisite for the high electronic dimensionality that is necessary for superior carrier transport.[7] In this regard, it is highly desirable for the light emitters to have a high luminescence efficiency while retaining a high structural dimensionality.

An important lesson learned from Sb^{3+}-based ternary iodides (with a formula $A_3Sb_2I_9$) is that variation of *A*-site cation will change not only optoelectronic properties of the compounds but also may dictate the structures that can be formed.[23] Herein, by employing a fluorinated organic spacer, we developed a facile cooling-induced crystallization protocol to produce 2D layered emissive Cu^+ metal halides, (DFPD)CuX_2 ($DFPD^+$ = 4,4-difluoropiperidinium, X^- = Cl^-, Br^-). Single-crystal X-ray diffraction (SCXRD) analyses confirm that (DFPD)CuX_2 consists of 2D-connected framework of $[CuX_4]^{3-}$ tetrahedra and charge-balancing $DFPD^+$. Density functional theory (DFT) calculations suggest that the conduction band of (DFPD)$CuBr_2$ exhibits

enhanced dispersive characteristics with a small effective mass, which is beneficial for efficient electrical injection. Additionally, (DFPD)CuX_2 single crystals exhibited excellent crystallinity and improved ambient stability, maintaining stable luminescence for over one month's storage in ambient air (RH ~40%, 30 °C), superior to the previously reported 0D $(MA)_2CuCl_3$, which is prone to hydrolytic damage.[20]

Results and Discussion

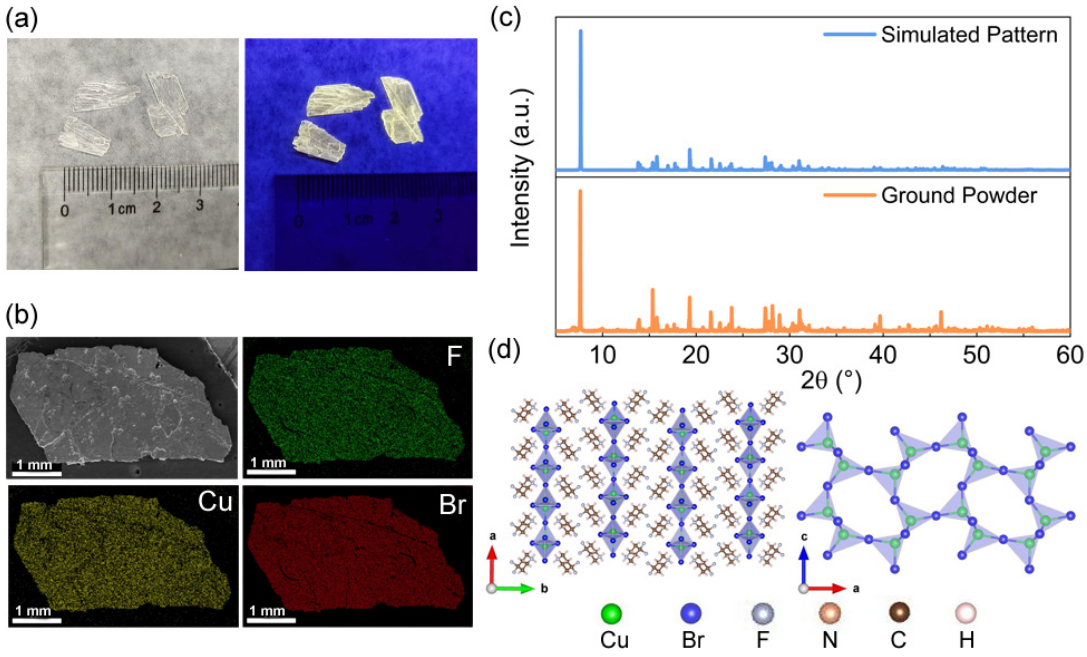

Figure 1. (a) Photographs of the as-prepared single crystals taken under visible (left)- and UV-light (right). (b) Element distribution analysis of (DFPD)$CuBr_2$ by EDS mapping. (c) Powder XRD pattern simulated and experimentally determined for the as-prepared single crystal. (d) Crystal structure of (DFPD)$CuBr_2$, created with VESTA software. Crystal information file (cif) is supplied in SI.

First, we will illustrate the synthesis results obtained for DFPD-Cu-Br system. Off-stoichiometric reactions were carried out in a hydrobromic media, which contains 4,4-difluoropiperidine and CuBr. Slow cooling of such a hot solution produces single crystals that present as 1-cm-wide and 0.2-cm-thick plates (see experimental details in Supporting Information, SI). To the naked eye, the crystals emit bright yellow light

under 254 nm UV light excitation (Figure 1a). Elemental mapping image (Figure 1b) obtained from energy dispersive X-ray spectroscopy (EDS) displays that the F, Cu, and Br elements are uniformly distributed in the crystal with molar ratio of 2.3:1:1.9 (Figure S1). SCXRD studies verify that the resulting crystals have molecular formula of (DFPD)$CuBr_2$, in good line with the EDS results. Powder XRD pattern acquired for the ground (DFPD)$CuBr_2$ single crystals shows the same feature as the simulated one, suggesting that the as-synthesized single crystals have a high degree of purity and uniformity (Figure 1c). The crystals crystallize in the orthorhombic *Pnma* space group and feature a 2D structure (crystallographic details and structure refinement of the crystals can be found in Figure 1d and Table S1-7). In such a crystal motif, each $[CuX_4]^{3-}$ tetrahedron is connected with three neighboring tetrahedra, one of which is through an edge-sharing way and the other two are through a corner-sharing way, forming a closely connected network in two directions. This 2D connection of inorganic polyhedra well explains the plate-like morphology of the obtained crystals. We may also note that such 2D structure is rarely seen in those of traditional Cu^+-based ternary halides, even in most of the reported Pb-free perovskites and their derivatives, including the recently reported Bi^{3+}-, Sb^{3+}-, In^{3+}-, and Ag^+-based metal halides, which usually feature a 0D structure.[20, 24-26]

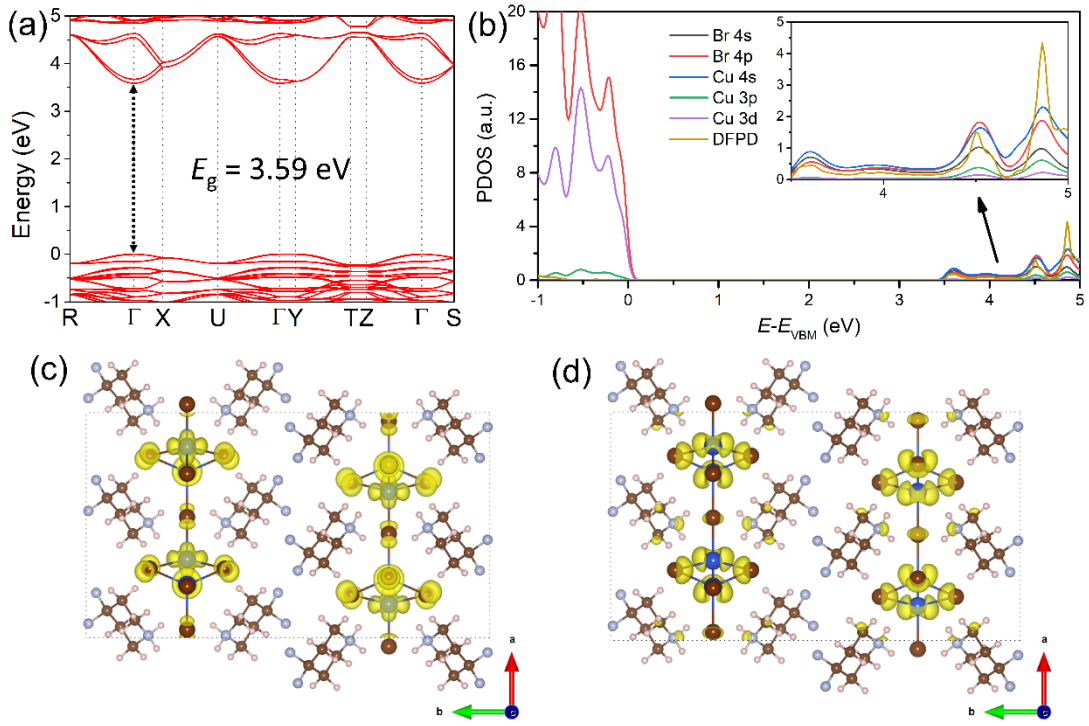

Figure 2. (a) Calculated band structure, (b) PDOS, and diagrams of the partial charge density for the (c) VBM and (d) CBM of (DFPD)$CuBr_2$. The isosurface value is 0.001 e $Å^{-3}$. DFT calculations are performed at the PBE level including Spin-orbit-coupling and a Hubbard correction of 10 eV to the Cu d states has been added to compute the band structure and PDOS (see SI for details).

To check whether this structure is unique to Br composition, we further conducted contrast synthesis by halide substitution. As expected, the Cl composition also allows the formation of 2-D connected $[CuCl_4]^{3-}$ tetrahedra that constitute the orthorhombic (DFPD)$CuCl_2$, which emits bright orange light under 254 nm UV light excitation (Figure S2, Table S8-14). The 2D connectivity of $[CuX_4]^{3-}$ inorganic framework provides a prerequisite for the charges to move in two directions if they are confined or generated in these tetrahedral layers.[27] To examine the electronic dimensionality of (DFPD)CuX_2, electronic band structure calculations based on DFT were performed. The calculated band structure of (DFPD)$CuBr_2$ indicates the material has a direct band gap transition with a bandgap (E_g) of ~3.59 eV (Figure 2a), close to that of the experimental value of 3.67 eV, as will be shown later. Note that the calculated E_g value

is largely influenced by the value set for the Hubbard parameter, see Table S15. We note that the direct character is similar to other Cu^{+}-based halides, such as $(MA)_2CuCl_3$, (TBA)$CuBr_2$, and $CsCu_2I_3$.[11, 20, 21, 28] Moreover, CBM of (DFPD)$CuBr_2$ has enhanced dispersive characteristics with a small effective mass of 0.17 m_0 along the Γ-X, 0.40 m_0 along the Γ-Y, and 0.18 m_0 along Γ-Z, respectively. The projected density of states (PDOS) shows that the VBM of (DFPD)$CuBr_2$ is hardly dispersed and composed mainly from Cu 3d and Br 4p orbitals, while the CBM is mainly formed by Br 4p and Cu 4s orbitals (Figure 2b), as indicated by the partial charge density (Figure 2c-d). The reliability of the organic/inorganic state alignment was further confirmed by measuring the energy levels of the DFPD-Br ligand and the (DFPD)$CuBr_2$ compound by ultraviolet photoelectron spectroscopy (UPS) and optical absorption measurements, see more details in Supporting Discussion 1. This result suggests that the band edges of (DFPD)$CuBr_2$ are mainly determined by the $[CuX_4]^{3-}$ tetrahedra. As noted above, this band structure will prospectively allow the injected or photogenerated charge carriers (electrons) to move in 2D. Overall, the above calculation shows (DFPD)$CuBr_2$ structure in high anisotropy with superior lateral charge transport.

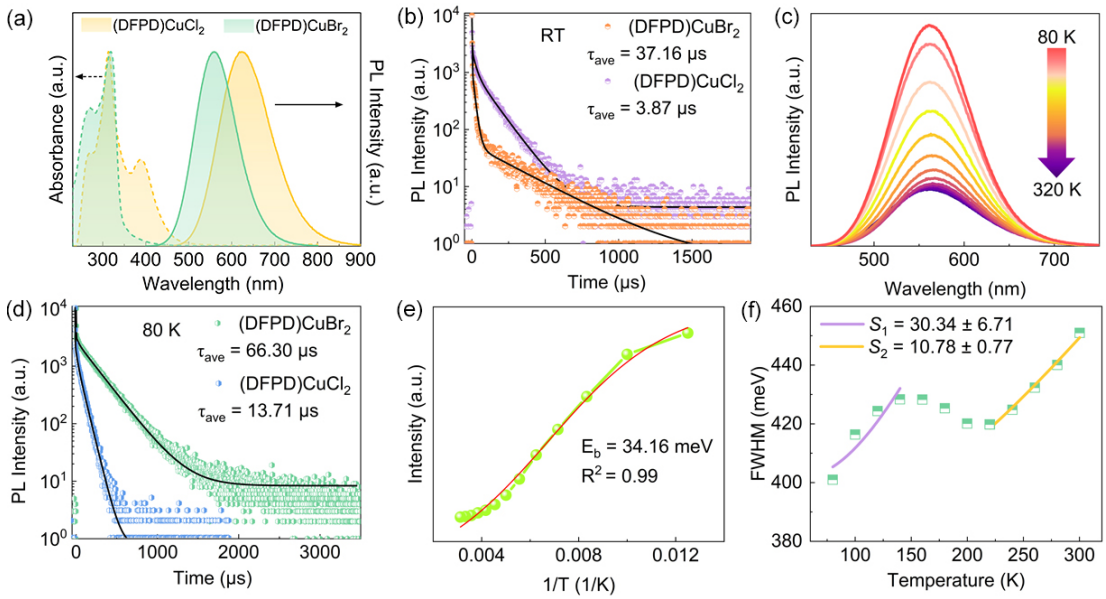

Figure 3. (a) UV-vis absorption, PL spectra, and (b) PL decay curves of the (DFPD)CuX_2 crystals, measured at 300 K. (c) Temperature-dependent PL spectra of

(DFPD)$CuBr_2$ measured from 320 to 80 K. (d) PL decay curves of the (DFPD)CuX_2 crystals, measured at 80 K. (e) Integrated PL intensity as a function of inverse temperature for (DFPD)$CuBr_2$. Data were fitted by using the Arrhenius equation.[29] (f) FWHM as a function of temperature.

Optical properties of the resulting crystals were investigated firstly by measuring their UV-vis absorption and PL spectra. (DFPD)$CuBr_2$ and (DFPD)$CuCl_2$ crystals present a sharp-edge absorption rising at 350 and 450 nm, respectively (Figure 3a), which coincides well with the predicted direct transition computed for (DFPD)$CuBr_2$ (Figure 2a). Figure S3 shows the Tauc's plot for the (DFPD)$CuBr_2$ sample, from which an E_g of 3.67 eV was extracted assuming direct band gap optical transitions. The PL excitation (PLE) spectra shown in Figure S4 determine the optimal excitation wavelength for each sample. Under optimal excitation conditions, PL spectra of both samples exhibit a broadband emission, characterized by large full width at half-maximum (FWHM) (Br: 0.48 eV, Cl: 0.51 eV) and large Stokes shifts (Br: 1.56 eV, Cl: 1.1 eV). Figure S5 presents the corresponding Commission Internationale de l'Eclairage (CIE) color coordinates and correlated color temperature (CCT) for each sample. It is important to note that (DFPD)$CuBr_2$ exhibits CCT value around 3761 K, which falls well in the warm white region of the spectrum (CCT around 2700 to 4000 K), thereby they can serve as a potential candidate for warm white LEDs (warm-WLEDs). We stress that there are not many single-component materials that could emit the warm white light.[20, 30] To examine how carriers recombine in the crystals, time-resolved PL (TRPL) measurements were performed. Figure 3b shows that the PL decay dynamics recorded for Cl- and Br-crystals follow triple-exponential statistics (fitting parameters were summarized in Table S16), suggestive of the presence of nonradiative pathways, in accordance with their non-unity PLQY.

To gain more insight into the effect of structural changes on luminescence properties of (DFPD)$CuBr_2$, temperature-dependent PL measurement was further

conducted. It is found that the broadband emission from 450 to 700 nm gradually increases in intensity with decreasing temperature from 320 to 80 K, accompanied by a prolonged radiative lifetime (Figure 3c-d). One possible explanation is that at lower temperatures, the thermal energy of the system decreases, leading to reduced molecular vibrations and less non-radiative decay processes.[21, 31] By fitting the derived PL intensity with temperature (Figure 3e), the exciton binding energy (E_b) was estimated to be 34 meV, smaller than most 0D metal halides which have large binding energies of several hundreds of meV.[32-34] This suggests a weakened exciton confinement in our crystals. We note that the experimentally determined non-unity PLQY exhibits potential correlations with this weakened electronic confinement featured in 2D structure as it diminishes local charge-charge interactions and leaves the carriers more vulnerable to the trap states.[14, 35, 36] Another experimental parameter that can be determined from temperature-dependent PL measurement is the well-known Huang-Rhys factor (S), which serves to evaluate the strength of electron-phonon coupling in the crystals. Generally, according to the magnitude of S, the electron-phonon coupling can be divided into extremely weak ($S < 1$), medium ($S = 1\sim5$), and strong ($S > 5$) zones. To gauge the effect of the electron-phonon coupling in our crystals, S value was obtained by using the following equation:

$$FWHM = 2.36\sqrt{S}\hbar\omega_{phonon}\sqrt{\coth\frac{\hbar\omega_{phonon}}{2k_BT}} \quad (1)$$

where $\hbar\omega_{phonon}$ is the effective phonon frequency and k_B the Boltzmann constant. FWHM data, derived from the temperature-dependent PL spectra are plotted in Figure 3f. Unexpectedly, unlike most other semiconductors, such as Ag^+-, In^{3+}-, Cd^{2+}-, and Cu^+-based compounds,[20] whose FWHM changes monotonously with increasing temperature, it is seen that the variation of FWHM of (DFPD)$CuBr_2$ is multistage. Usually, FWHM increases with increasing temperature as a result of an enhanced optical phonon scattering, however, FWHM of (DFPD)$CuBr_2$ shows a gradual decline in the temperature range from 150 to 200 K. Piecewise nonlinear fitting of the curve using equation 1 reveals that (DFPD)$CuBr_2$ crystal has S factor of 30 ± 7 in the

temperature range from 100 to 150 K and $S = 11 \pm 1$ from 200 to 300 K. This variation in S value characterizes a temperature-associated change in exciton-phonon coupling. To rule out the potential phase change with temperature, we performed additional SCXRD analysis at 300 K and compared the results to that obtained at 150 K. Crystallographic details and structure refinement (see Table S1 and S17) show that both the phase and lattice parameters of the crystals remain intact when decreasing temperature from 300 to 150 K, suggesting that the temperature variation has little impact on their crystal structure. The smaller S value at higher temperatures reminds us of a similar observation reported by Xu *et al.*, where the exciton-phonon coupling in $CsPbBr_3$ nanosheets thermally diminishes in the temperature range from 5 to 40 K.[37] This behavior is ascribed to the effect of dielectric confinement because the Huang-Rhys factor is closely related to static dielectric constant of the semiconductor,[3] which can be a strong function of temperature.[38-40] Complex behavior such as negative thermal quenching has also been observed for more regular halide perovskites such as $FASnI_3$.[41] In this case, the effect depends on the sample preparation and defect content, and may result from the suppression of non-radiative recombination pathways in samples of high quality. Alternatively, the interplay between the formation of bound and free exciton states shall be considered.

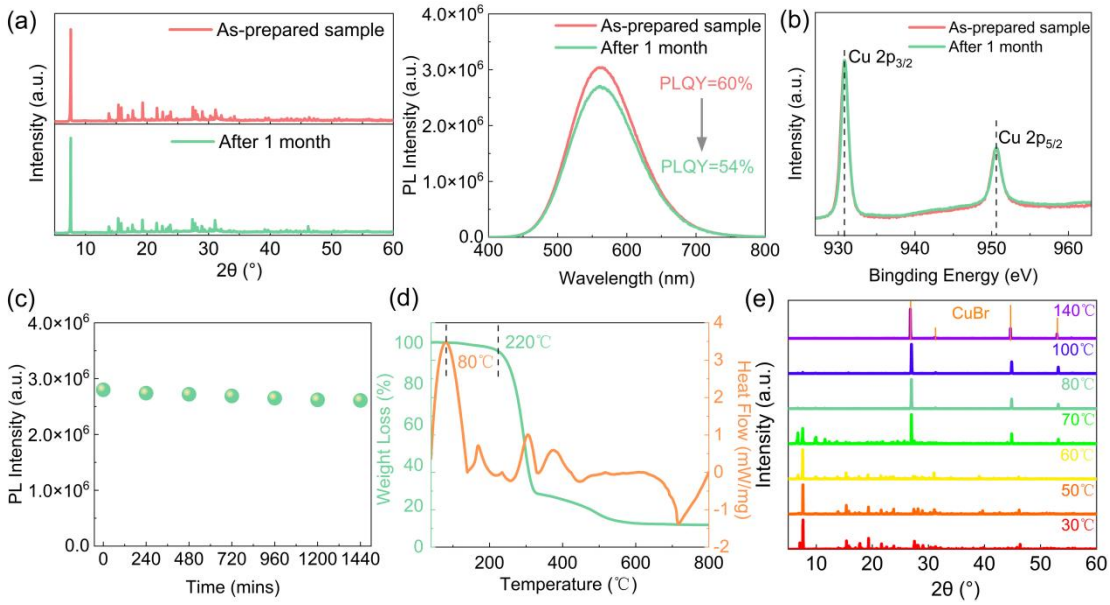

Figure 4. (a) XRD patterns, PL spectra, and (b) high-resolution Cu 2p XPS spectra measured for the freshly-prepared samples and those after 1-month storage in ambient air. (c) Time-resolved PL intensity (monitored at 565 nm) of the (DFPD)$CuBr_2$ single crystals with continuous irradiation of 254 nm light for 24 h. Note that the irradiation experiment was conducted in a nitrogen gas-filled glove box. (d) TG-DSC curves and (e) variable-temperature XRD patterns of (DFPD)$CuBr_2$ single crystals.

Structural and optical stabilities of a luminescent material are of paramount importance for assessing their suitability for light-emitting applications. It should be noted that the previously reported 0D-structured $(MA)_2CuCl_3$ exhibited a similar warm white-light emission as (DFPD)$CuBr_2$. However, $(MA)_2CuCl_3$ has a poor ambient stability because of its high hygroscopicity.[20] To evaluate the ambient stability of (DFPD)$CuBr_2$, powder XRD measurement was firstly carried out. Figure 4a shows that the crystal structure of (DFPD)$CuBr_2$ remains intact even after 1-month storage in ambient air (RH ~40%, 30 °C), along with the retention of the appealing broadband emission and PLQY. This result points to an improved ambient stability of (DFPD)$CuBr_2$. We consider this is from the non-negligible covalent characteristics of Cu-Br bonds as suggested by DFT calculations (Figure S6), which weakens ionic nature and thus endows the compound with better hydrophobicity. X-ray photoelectron spectroscopy (XPS) was further performed to confirm the presence of Cu element in its original oxidation state. Figure 4b displays that the Cu XPS spectrum of the aged sample matches well with that of the as-prepared one, confirming that the (DFPD)$CuBr_2$ single crystals have a high resistance against oxidation. Photostability of the (DFPD)$CuBr_2$ single crystals was also evaluated as it is closely related to their light-emitting applications. Figure 4c shows that the crystal retains almost 95% of the initial PL intensity after a continuous irradiation of 254 nm light for over 24 h, which suggests an excellent light stability. Thermal stability of the crystals was next evaluated by thermogravimetric (TG) analysis. Figure 4d shows that the decomposition of the material occurs at around 220 °C, which loses ~60% of its initial mass at 300 °C,

presumably due to the evaporation of the comprised organics. However, before material decomposition, it is noticed from the differential scanning calorimetry (DSC) curve that (DFPD)$CuBr_2$ crystals may have undergone a melting process, as evidenced by the obvious endothermic peak at 80 °C. To investigate the possible phase change during heat treatment, variable-temperature XRD measurement was carried out. It is seen that the main diffraction peaks of the (DFPD)$CuBr_2$ single crystals remain almost constant in the temperature range from 30 to 60 °C (Figure 4e). With continuous heating to 100 °C, diffraction peaks assignable to CuBr dominate the diffraction pattern, accompanied by a complete loss of PL (Figure S7), indicating a significant phase change at elevated temperatures. However, we also note that this melting process is reversible, that is, the solid (DFPD)$CuBr_2$ compound can be mostly recovered upon cooling from 100 °C to room temperature, along with their bright PL, exhibiting the reusability of such materials.

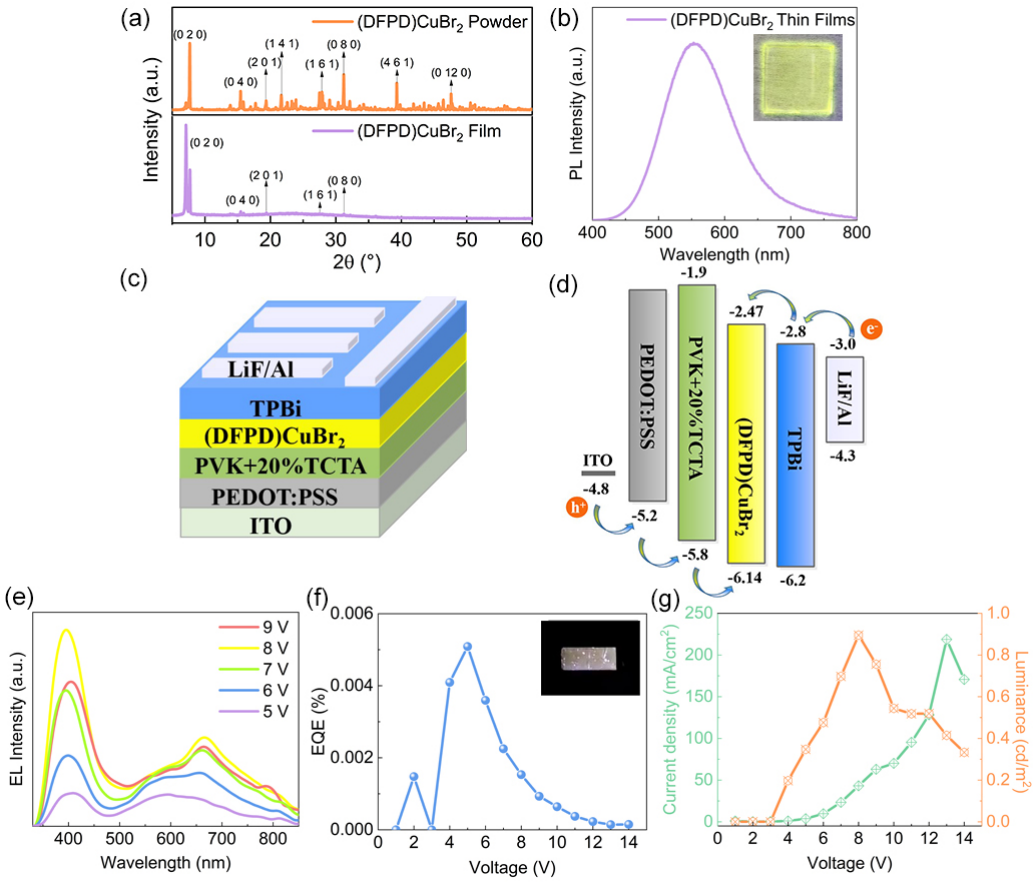

Figure 5. (a) XRD pattern and (b) PL spectrum of (DFPD)$CuBr_2$ thin films. Inset shows

a photograph of a typical thin film sample taken under 254 nm UV light. (c) Schematic illustration of the best-performing LED devices. (d) Energy level diagram for the device structure. UPS which determines the valence band maximum (VBM) of the emitters is presented in Figure S8. (e) EL spectra of the best-performing LEDs under different bias voltages. (f) Continuous-wave EQE (Inset: photograph of the LED driven by a 7 V bias) and (g) *J-V-L* characteristics of the LED devices.

The 2D character, high phase stability, and warm white-light emission properties make the (DFPD)$CuBr_2$ material attractive for WLED applications. To incorporate luminescent materials into electrically driven LEDs, the first step involves transforming these bulk crystals into dense thin films, thereby facilitating efficient charge injection. We observe that while thin films of Pb-based halide perovskites can be readily deposited using solution-based methods, a major obstacle in the widespread adoption of these "perovskite-inspired" materials in optoelectronics lies in the absence of an appropriate solvent capable of dissolving them for solution processing. The commonly used coordinating solvents, such as N,N-dimethylformamide (DMF) and dimethylsulfoxide (DMSO), were found to be capable of dissolving (DFPD)$CuBr_2$, but the obtained solutions gradually turned from colorless to green, indicative of Cu^+ oxidation (Figure S9). In our previous demonstration of $(MA)_2CuCl_3$ thin films, methanol solvent was employed to dissolve $(MA)_2CuCl_3$.[16] But we found poor solubility of (DFPD)$CuBr_2$ in methanol, which prevents the fabrication of (DFPD)$CuBr_2$ thin films by the same protocol. We note that the low solubility of (DFPD)$CuBr_2$ in methanol is consistent with its high stability in ambient conditions, which is believed to be attributed to the non-negligible covalent nature of Cu-Br bonds. To achieve functional thin films, 1-methoxy-2-propanol (M2P) was proposed. M2P shows good solvation ability, and importantly, no sign of Cu^+ oxidation is observed (Figure S10). Spin coating of M2P solution followed by heat treatment at 50 °C allows the successful deposition of (DFPD)$CuBr_2$ thin films on glass substrate. XRD pattern of the prepared thin films evidences the recovery of pure-phase 2D (DFPD)$CuBr_2$

(Figure 5a), whose PL spectrum resembles that of the single-crystal structures (Figure 5b).

The M2P-based deposition process enables us to fabricate electrically driven LEDs by a low-cost solution way. The device structure employed here is indium-tin oxide (ITO) glass/poly(3,4-ethylenedioxythiophene):poly(styrenesulfonate) (PEDOT:PSS)/poly(9-vinlycarbazole) (PVK)+20% tris(4-carbazoyl-9-ylphenyl)amine (TCTA)/(DFPD)$CuBr_2$/2,2′,2″-(1,3,5-benzenetriyl)tris-(1-phenyl-1H-benzimidazole) (TPBi)/lithium fluoride (LiF)/aluminum (Al) (Figure 5c) (details about the device fabrication can be found in SI). The alignment of energy levels can be seen in Figure 5d. As the applied voltage increases, an appreciable white-light (or yellow) emission was seen from the LED device, indicating that charge carriers were injected and recombined in the (DFPD)$CuBr_2$ layers. To the best of our knowledge, this represents the first successful demonstration of EL from 2D Cu^+ metal halides. Video S1 in SI records the real-time measurement of a typical device with voltage scanning. Figure 5e shows EL spectra of the LEDs, which have almost the same emission feature at different applied biases from 5 to 9 V. However, in addition to (DFPD)$CuBr_2$ emission in the wavelength range of 450~800 nm, we also observed parasitic emission around 400 nm, which can be assigned to neighboring PVK layers (more characterizations about this assignment can be found in Figure S11). As discussed later, this can be caused by the incomplete coverage of the (DFPD)$CuBr_2$ films on PVK. CIE chromaticity coordinates of the LEDs are given in Figure S12, where both signals of (DFPD)$CuBr_2$ and PVK can be resolved. Figure 5f-g present the continuous-wave EQE curve and current-voltage-luminance (*J-V-L*) characteristics of the LEDs. The LED exhibits a maximum luminance ~0.9 cd/m^2 and an EQE of 0.005%.

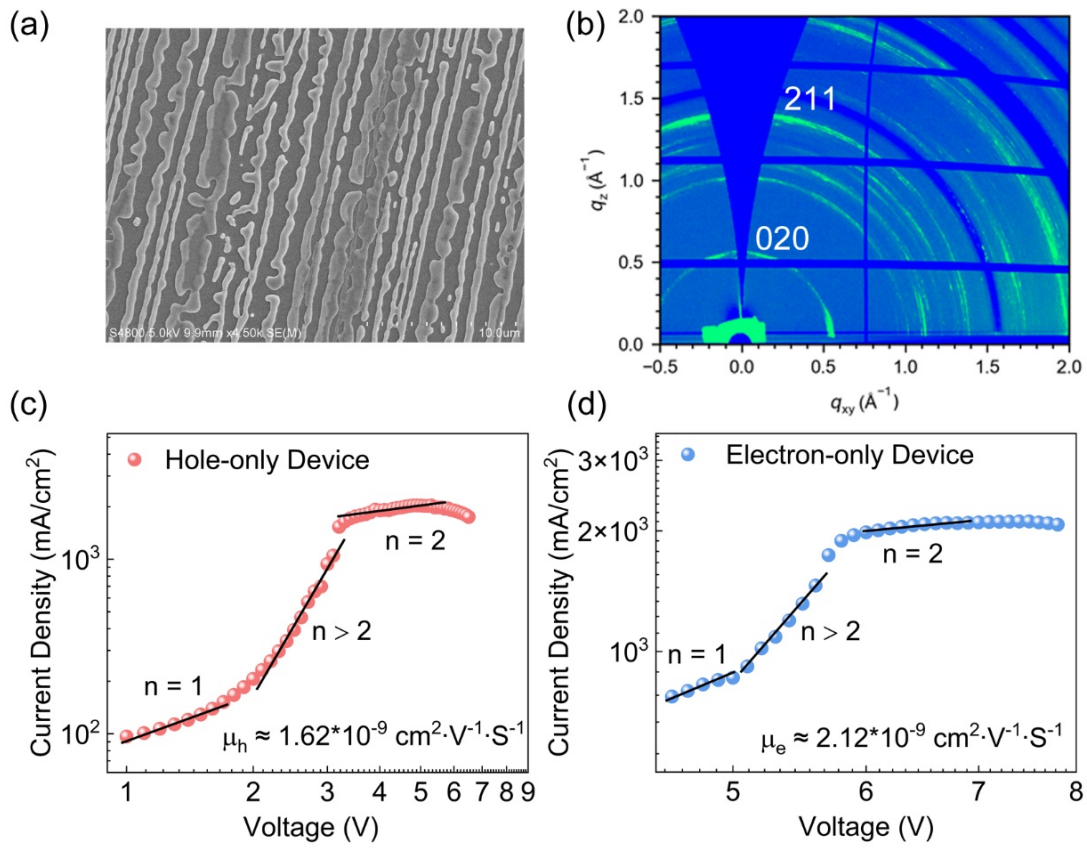

Figure 6. (a) Plane-view SEM image of a typical thin film sample. (b) GIWAXS pattern of (DFPD)$CuBr_2$ thin films. (c) Current density versus voltage for hole-only and (d) electron-only device.

Based on the 2D structure of pure materials, we would anticipate improved EL performance from thin films of (DFPD)$CuBr_2$. However, the achieved device efficiency falls short compared to the 0D MA_2CuCl_3 LEDs (EQE ~0.04%) and 1D (DFPD)KInBr:Sb (EQE ~0.46%).[20, 42] To learn the underlying reasons for this, morphology of the emissive layers was first investigated by scanning electron microscopy (SEM) analysis. The plane-view SEM image of a typical (DFPD)$CuBr_2$ thin film sample indicates that, despite the strong solvation ability of M2P, the deposited films are discontinuous in nature and consist of separate clusters or islands on the substrate surface (Figure 6a). This lack of compactness will cause large leakage currents and thus deteriorate the LED performance. Further, we assessed the crystallographic orientation with respect to the substrate in the thin films using grazing incidence wide-

angle X-ray scattering (GIWAXS) measurements. It is found that the (DFPD)$CuBr_2$ films exhibit diffraction rings with stronger intensities along certain extended arc segments (Figure 6b), which indicates formation of (DFPD)$CuBr_2$ crystals without preferred orientation. Such randomness in the orientation of the crystal grains would possess unfavorable effect on charge transporting characteristic in thin films, as it allows for both in-plane and out-of-plane charge transport directions.[43, 44] To examine the charge mobility (μ) in (DFPD)$CuBr_2$ thin films, space-charge-limited current measurement was performed. Hole-only devices were fabricated using the structure ITO/PEDOT:PSS/(DFPD)$CuBr_2$/TCTA/Ag; electron-only devices were fabricated using the structure ITO/ZnO/(DFPD)$CuBr_2$/TPBi/LiF/Al. Figure 6c-d show the corresponding *J-V* curve in dark condition. The electron mobility (μ_e) and hole mobility (μ_h) of the thin films can be extracted by fitting the Child's regime with the Mott-Gurney law:

$$J = \frac{9\varepsilon\mu\varepsilon_0 V^2}{8d^3} \quad (2)$$

where V is the applied voltage, J is the current density, ε is the relative dielectric permittivity of (DFPD)$CuBr_2$ and ε_0 is the vacuum dielectric permittivity, d is the thickness of the film, which is estimated to be ~85 nm from the SEM image (Figure S13). From the fit to our data, μ_h value was extracted to be 1.62×10^{-9} $cm^2/V{\cdot}s$ and μ_e to be 2.12×10^{-9} $cm^2/V{\cdot}s$, both are three orders of magnitude lower than that of (DFPD)KInBr:Sb perovskite.[42] We consider the low electron mobility could be attributed to electron hopping rather than band conduction. Optical properties of the resulting (DFPD)$CuBr_2$ thin films were next evaluated by measuring their PLQYs. We found PLQY of the deposited films significantly decreased to 19%, much lower than that of MA_2CuCl_3 (~90%) and (DFPD)KInBr:Sb (~50%). Other significant factors leading to the limited efficiency of present LEDs include the high conduction band position of (DFPD)$CuBr_2$ (Figure 5d), which hampers electron injection efficiency and exacerbates the challenge of energy conversion inefficiency. Further research is required to optimize the morphology of (DFPD)$CuBr_2$ thin films, improve the PLQY, and refine device design for enhanced performance.

Conclusions

We report the first example of 2D layered Cu^{+}-based metal halide, (DFPD)CuX_2, which exhibits unique high-dimensional tetrahedral connectivity relative to previously reported 0D/1D metal halides. Theoretical calculations confirm electronic dimensionality of these Cu^{+}-based metal halides increases as a result of the increased structural dimension, making it possible for the materials to achieve a higher charge mobility. Furthermore, the obtained 2D (DFPD)$CuBr_2$ single crystals show bright warm white-light emission with an outstanding ambient stability, being a promising candidate for single-component lighting and display applications. To showcase the practicality of these luminescent compounds in electron-driven devices, we further devised a solution-based approach to depositing (DFPD)CuX_2 thin films, which exhibited promising EL in WLEDs. However, further improvements are urgently needed regarding the film morphology.

Associated Content

Supporting Information

X-ray crystallographic files, experimental and computational details, UV-vis absorption spectra, EDS, UPS spectrum, SEM image, EL spectra of the LED, CIE color coordinates, XRD patterns.

Corresponding Authors

*E-mails: jacky.even@insa-rennes.fr (J. Even); fenglau189@sdu.edu.cn (F. Liu); wyu6000@gmail.com (W. W. Yu)

Notes

The authors declare no competing financial interest.

Acknowledgements

This work was financially supported by the National Natural Science Foundation of China (22179072, 62374104), the Natural Science Foundation of Shandong Province (ZR2021QF006), the Outstanding Youth Science Foundation of Shandong Province (Overseas) (2022HWYQ-006), and the Qilu Youth Scholar Foundation of Shandong University (62460082163114). The work at Rennes acknowledges funding from the M-ERA.NET project PHANTASTIC (R.8003.22), funding from Région Bretagne, the European Union's Horizon 2020 program, through an Innovation Action under Grant Agreement No. 861985 (PeroCUBE) and through a FET Open research and innovation action under the Grant Agreement No. 899141 (PoLLoC). J.E. acknowledges the financial support from the Institut Universitaire de France. This work was granted access to the HPC resources of TGCC under the allocations 2022-A0110907682 made by GENCI.

References

1. Kojima A., Teshima K., Shirai Y. and Miyasaka T., Organometal Halide Perovskites as Visible-Light Sensitizers for Photovoltaic Cells. *J. Am. Chem. Soc.*, 2009, **131**, 6050-6051.
2. Zhao Y., Ma F., Qu Z., Yu S., Shen T., Deng H.-X., Chu X., Peng X., Yuan Y., Zhang X. and You J., Inactive (PbI2)2RbCl Stabilizes Perovskite Films for Efficient Solar Cells. *Science*, 2022, **377**, 531-534.
3. Best Research-Cell Efficiency Chart. https://www.nrel.gov/pv/cell-efficiency.html.
4. Jiang J., Chu Z., Yin Z., Li J., Yang Y., Chen J., Wu J., You J. and Zhang X., Red Perovskite Light-Emitting Diodes with Efficiency Exceeding 25% Realized by Co-Spacer Cations. *Adv. Mater.*, 2022, **34**, 2204460.
5. Bai W., Xuan T., Zhao H., Dong H., Cheng X., Wang L. and Xie R.-J., Perovskite Light-Emitting Diodes with an External Quantum Efficiency Exceeding 30%. *Adv. Mater.*, 2023, **35**, 2302283.

6. Yuan S., Dai L., Sun Y., Auras F., Zhou Y.-H., An R.-Z., Liu Y., Ding C., Cassidy C., Tang X., Dong S.-C., Kang H.-B., Chen K., Liu X., Ye Z.-F., Zhao Y., Adachi C., Liao L.-S., Greenham N. C., Qi Y., Stranks S. D., Cui L.-S. and Friend R. H., Efficient Blue Electroluminescence from Reduced-Dimensional Perovskites. *Nat. Photonics*, 2024, DOI: 10.1038/s41566-024-01382-6.

7. Zhao X.-G., Yang D., Ren J.-C., Sun Y., Xiao Z. and Zhang L., Rational Design of Halide Double Perovskites for Optoelectronic Applications. *Joule*, 2018, **2**, 1662-1673.

8. Even J., Pedesseau L., Katan C., Kepenekian M., Lauret J.-S., Sapori D. and Deleporte E., Solid-State Physics Perspective on Hybrid Perovskite Semiconductors. *J. Phys. Chem. C*, 2015, **119**, 10161-10177.

9. Wang A., Zuo C., Niu X., Ding L., Ding J. and Hao F., Recent Promise of Lead-Free Halide Perovskites in Optoelectronic Applications. *Chem. Eng. J.*, 2023, **451**, 138926.

10. Cui W., Zhao J., Wang L., Lv P., Li X., Yin Z., Yang C. and Tang A., Unraveling the Phase Transition and Luminescence Tuning of Pb-Free Cs–Cu–I Perovskites Enabled by Reaction Temperature and Polar Solvent. *J. Phys. Chem. Lett.*, 2022, **13**, 4856-4863.

11. Ma Z., Ji X., Wang M., Zhang F., Liu Z., Yang D., Jia M., Chen X., Wu D., Zhang Y., Li X., Shi Z. and Shan C., Carbazole-Containing Polymer-Assisted Trap Passivation and Hole-Injection Promotion for Efficient and Stable CsCu2I3-Based Yellow LEDs. *Adv. Sci.*, 2022, **9**, 2202408.

12. Seo G., Jung H., Creason T. D., Yeddu V., Bamidele M., Echeverria E., Lee J., McIlroy D., Saparov B. and Kim D. Y., Lead-Free Halide Light-Emitting Diodes with External Quantum Efficiency Exceeding 7% Using Host–Dopant Strategy. *ACS Energy Lett.*, 2021, **6**, 2584-2593.

13. Li J., Yang L., Guo Q., Du P., Wang L., Zhao X., Liu N., Yang X., Luo J. and Tang J., All-Vacuum Fabrication of Yellow Perovskite Light-Emitting Diodes. *Sci. Bull.*, 2022, **67**, 178-185.

14. Jun T., Sim K., Iimura S., Sasase M., Kamioka H., Kim J. and Hosono H., Lead-Free Highly Efficient Blue-Emitting Cs3Cu2I5 with 0D Electronic Structure. *Adv. Mater.*, 2018, **30**, 1804547.

15. Zhang F., Zhao Z., Chen B., Zheng H., Huang L., Liu Y., Wang Y. and Rogach A. L., Strongly Emissive Lead-Free 0D Cs3Cu2I5 Perovskites Synthesized by a Room Temperature Solvent Evaporation Crystallization for Down-Conversion Light-Emitting Devices and Fluorescent Inks. *Adv. Optical Mater.*, 2020, **8**, 1901723.

16. Wang L., Shi Z., Ma Z., Yang D., Zhang F., Ji X., Wang M., Chen X., Na G., Chen S., Wu D., Zhang Y., Li X., Zhang L. and Shan C., Colloidal Synthesis of Ternary Copper Halide Nanocrystals for High-Efficiency Deep-Blue Light-Emitting Diodes with a Half-Lifetime above 100 h. *Nano Lett.*, 2020, **20**, 3568-3576.

17. Li J., Inoshita T., Ying T., Ooishi A., Kim J. and Hosono H., A Highly Efficient and Stable Blue-Emitting Cs5Cu3Cl6I2 with a 1D Chain Structure. *Adv. Mater.*, 2020, **32**, 2002945.

18. Huang J., Su B., Song E., Molokeev M. S. and Xia Z., Ultra-Broad-Band-Excitable Cu(I)-Based Organometallic Halide with Near-Unity Emission for Light-Emitting Diode Applications. *Chem. Mater.*, 2021, **33**, 4382-4389.

19. Zhou L., Liao J.-F. and Kuang D.-B., An Overview for Zero-Dimensional Broadband Emissive Metal-Halide Single Crystals. *Adv. Optical Mater.*, 2021, **9**, 2100544.

20. Meng X., Ji S., Wang Q., Wang X., Bai T., Zhang R., Yang B., Li Y., Shao Z., Jiang J., Han K.-l. and Liu F., Organic–Inorganic Hybrid Cuprous-Based Metal Halides for Warm White Light-Emitting Diodes. *Adv. Sci.*, 2022, **9**, 2203596.

21. Lian L., Wang X., Zhang P., Zhu J., Zhang X., Gao J., Wang S., Liang G., Zhang D., Gao L., Song H., Chen R., Lan X., Liang W., Niu G., Tang J. and Zhang J., Highly Luminescent Zero-Dimensional Organic Copper Halides for X-ray Scintillation. *J. Phys. Chem. Lett.*, 2021, **12**, 6919-6926.

22. Xiao Z., Du K.-Z., Meng W., Mitzi D. B. and Yan Y., Chemical Origin of the Stability Difference between Copper(I)- and Silver(I)-Based Halide Double Perovskites. *Angew. Chem. Int. Ed.*, 2017, **56**, 12107-12111.

23. Correa-Baena J.-P., Nienhaus L., Kurchin R. C., Shin S. S., Wieghold S., Putri Hartono N. T., Layurova M., Klein N. D., Poindexter J. R., Polizzotti A., Sun S., Bawendi M. G. and Buonassisi T., A-Site Cation in Inorganic A3Sb2I9 Perovskite Influences Structural Dimensionality, Exciton Binding Energy, and Solar Cell Performance. *Chem. Mater.*, 2018, **30**, 3734-3742.

24. Tewari N., Shivarudraiah S. B. and Halpert J. E., Photorechargeable Lead-Free Perovskite Lithium-Ion Batteries Using Hexagonal Cs3Bi2I9 Nanosheets. *Nano Lett.*, 2021, **21**, 5578-5585.

25. Sun S., Lu M., Gao X., Shi Z., Bai X., Yu W. W. and Zhang Y., 0D Perovskites: Unique Properties, Synthesis, and Their Applications. *Adv. Sci.*, 2021, **8**, 2102689.

26. Ji S., Meng X., Wang X., Bai T., Zhang R., Yang B., Han K., Jiang J. and Liu F., Colloidal Synthesis of Size-Confined CsAgCl2 Nanocrystals: Implications for Electroluminescence Applications. *Mater. Chem. Front.*, 2022, **6**, 3669-3677.

27. Li Z., Li Z., Shi Z. and Fang X., Facet-Dependent, Fast Response, and Broadband Photodetector Based on Highly Stable All-Inorganic CsCu2I3 Single Crystal with 1D Electronic Structure. *Adv. Funct. Mater.*, 2020, **30**, 2002634.

28. Lin R., Guo Q., Zhu Q., Zhu Y., Zheng W. and Huang F., All-Inorganic CsCu2I3 Single Crystal with High-PLQY (≈15.7%) Intrinsic White-Light Emission via Strongly Localized 1D Excitonic Recombination. *Adv. Mater.*, 2019, **31**, 1905079.

29. Laidler K. J., The Development of the Arrhenius Equation. *J. Chem. Educ.*, 1984, **61**, 494.

30. Luo J., Wang X., Li S., Liu J., Guo Y., Niu G., Yao L., Fu Y., Gao L., Dong Q., Zhao C., Leng M., Ma F., Liang W., Wang L., Jin S., Han J., Zhang L., Etheridge

J., Wang J., Yan Y., Sargent E. H. and Tang J., Efficient and Stable Emission of Warm-White Light From Lead-Free Halide Double Perovskites. *Nature*, 2018, **563**, 541-545.

31. Fang Z., He H., Gan L., Li J. and Ye Z., Understanding the Role of Lithium Doping in Reducing Nonradiative Loss in Lead Halide Perovskites. *Adv. Sci.*, 2018, **5**, 1800736.
32. Shi M., Li G., Tian W., Jin S., Tao X., Jiang Y., Pidko E. A., Li R. and Li C., Understanding the Effect of Crystalline Structural Transformation for Lead-Free Inorganic Halide Perovskites. *Adv. Mater.*, 2020, **32**, 2002137.
33. Zhang G., Wang D., Lou B., Ma C.-G., Meijerink A. and Wang Y., Efficient Broadband Near-Infrared Emission from Lead-Free Halide Double Perovskite Single Crystal. *Angew. Chem. Int. Ed.*, 2022, **61**, e202207454.
34. Zheng X., Huang J., Liu Y., Wang T., Han S., Wang Z., Teng B. and Ji S., Stable Lead-Free Blue-Emitting Cs3Cu2Br5 Single Crystal with Self-Trap Exciton Emission for Optoelectronics. *Adv. Photonics Res.*, 2022, **3**, 2100289.
35. Zhang D., Gu L., Zhang Q., Lin Y., Lien D.-H., Kam M., Poddar S., Garnett E. C., Javey A. and Fan Z., Increasing Photoluminescence Quantum Yield by Nanophotonic Design of Quantum-Confined Halide Perovskite Nanowire Arrays. *Nano Lett.*, 2019, **19**, 2850-2857.
36. Lin J.-T., Liao C.-C., Hsu C.-S., Chen D.-G., Chen H.-M., Tsai M.-K., Chou P.-T. and Chiu C.-W., Harnessing Dielectric Confinement on Tin Perovskites to Achieve Emission Quantum Yield up to 21%. *J. Am. Chem. Soc.*, 2019, **141**, 10324-10330.
37. Lao X., Yang Z., Su Z., Bao Y., Zhang J., Wang X., Cui X., Wang M., Yao X. and Xu S., Anomalous Temperature-Dependent Exciton–Phonon Coupling in Cesium Lead Bromide Perovskite Nanosheets. *J. Phys. Chem. C*, 2019, **123**, 5128-5135.
38. Nomura S. and Kobayashi T., Exciton--LO-Phonon Couplings in Spherical Semiconductor Microcrystallites. *Phys. Rev. B*, 1992, **45**, 1305-1316.

39. Cheng Z. Y., Katiyar R. S., Yao X. and Bhalla A. S., Temperature Dependence of the Dielectric Constant of Relaxor Ferroelectrics. *Phys. Rev. B*, 1998, **57**, 8166-8177.

40. Rupprecht G. and Bell R. O., Dielectric Constant in Paraelectric Perovskites. *Phys. Rev.*, 1964, **135**, A748-A752.

41. Kahmann S., Nazarenko O., Shao S., Hordiichuk O., Kepenekian M., Even J., Kovalenko M. V., Blake G. R. and Loi M. A., Negative Thermal Quenching in FASnI3 Perovskite Single Crystals and Thin Films. *ACS Energy Lett.*, 2020, **5**, 2512-2519.

42. Bai T., Wang X., Wang Z., Ji S., Meng X., Wang Q., Zhang R., Han P., Han K.-l., Chen J., Liu F. and Yang B., Highly Luminescent One-Dimensional Organic–Inorganic Hybrid Double-Perovskite-Inspired Materials for Single-Component Warm White-Light-Emitting Diodes. *Angew. Chem. Int. Ed.*, 2023, **62**, e202213240.

43. Liu C., Fang Z., Sun J., Lou Q., Ge J., Chen X., Zhou E., Shang M.-H., Yang W. and Ge Z., Imidazolium Ionic Liquid as Organic Spacer for Tuning the Excitonic Structure of 2D Perovskite Materials. *ACS Energy Lett.*, 2020, **5**, 3617-3627.

44. Niu T., Lu J., Jia X., Xu Z., Tang M.-C., Barrit D., Yuan N., Ding J., Zhang X., Fan Y., Luo T., Zhang Y., Smilgies D.-M., Liu Z., Amassian A., Jin S., Zhao K. and Liu S., Interfacial Engineering at the 2D/3D Heterojunction for High-Performance Perovskite Solar Cells. *Nano Lett.*, 2019, **19**, 7181-7190.

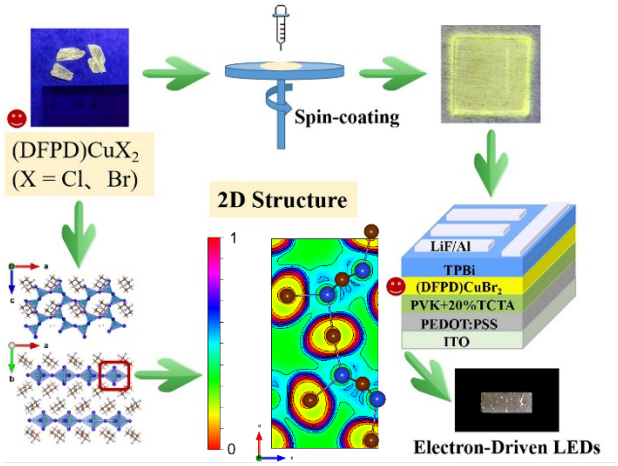
Spin-coating
(DFPD)CuX2
(X = Cl、 Br)
2D Structure
1
0
LiF/Al
TPBi
(DFPD)CuBr2
PVK+20%TCTA
PEDOT:PSS
ITO
Electron-Driven LEDs

TOC